J. Fluid Mech. (2007), *vol.* 582, *pp.* 133–151.
doi:10.1017/S0022112007005745 Printed in the United Kingdom

The merger of two-dimensional radially stratified high-Froude-number vortices

LAURENT JOLY[1] AND JEAN N. REINAUD[2]

[1]ENSICA, 1 Place Émile Blouin, 31056 Toulouse, France

[2]Mathematical Institute, University of St Andrews, KY16 9SS, St Andrews, UK

(Received 20 December 2005 and in revised form 10 January 2007)

We investigate the influence of density inhomogeneities on the merger of two co-rotating two-dimensional vortices at infinite Froude number. In this situation, buoyancy effects are negligible, yet density variations still affect the flow by pure inertial effects through the baroclinic torque. We first re-address the effects of a finite Reynolds number on the interaction between two identical Gaussian vortices. Then, by means of direct numerical simulations, we show that vortices transporting light fluid in a heavier counterpart merge from further distances than vortices in a uniform density medium. On the other hand, heavy vortices only merge from small separation distances. We measure the critical distance a/b_0 of the vortex radii to their initial separation distance. It departs from the homogeneous threshold of 0.22 in response to increasing density contrasts between the vortices and their surroundings. An analysis of the contribution of the baroclinic vorticity to the dynamics of the flow is detailed and explains the observed behaviour. This analysis is completed by a simple model based on point vortices that mimics the flow. It is concluded that vortices carrying light fluid are more likely to generate large-scale structures than heavy ones in an inhomogeneous fluid.

1. Introduction

Vortices – or swirling masses of fluid – are ubiquitous in nature and are the key dynamical features in many industrial and geophysical contexts. Hence, understanding how these structures interact is crucial to the understanding of many complex fluid flows. Vortex merger or more generally the strong interaction between two co-rotating two-dimensional vortices has been extensively studied. Previous studies first addressed the interaction between two uniform patches of vorticity in a homogeneous inviscid fluid. One of the first focuses of these studies was the determination of the margin of stability for a pair of vorticity patches in mutual equilibrium. The margin of stability, corresponding to a critical distance between the two vortices below which the flow becomes unstable, is associated with the critical merger distance as the instability may trigger a strong interaction between the two co-rotating vortices. This issue has been investigated by Saffman & Szeto (1980) and has been revisited in Dritschel (1995) and Cerretelli & Williamson (2003). On the other hand, numerical simulations based on contour advection (see Melander, Zabusky & McWilliams 1988; Dritschel & Waugh 1992; Waugh 1992; Dritschel 1995) were used to address the nonlinear evolution of the flow, illustrating its possible complexity with complete or partial merger or even only weak exchange of vorticity between the two vortices.

More recently, the interaction of distributed vortices has been examined. For example, Meunier *et al.* (2002) considered the interaction between two distributed

vortices both experimentally and theoretically, and Meunier, Le Dizès & Leweke (2005) illustrated the nonlinear evolution of such an interaction by direct numerical simulations. They concluded that the critical distance for distributed vortices and vortex patches to interact strongly might be written as a multiple of a length scale defined from the angular impulse and the circulation.

Most of these studies aimed to address one of the forms of vortex interaction observed in two-dimensional turbulence, in an attempt to explain in the physical space the 'inverse' energy cascade and the direct enstrophy cascade commonly observed in the spectral space. During the merger process, the creation of larger vortices feeds the large scales of the energy spectrum whereas the generation of low-energy filaments feeds the small scales of the enstrophy spectral distribution.

In this paper, we address the strong interaction between two two-dimensional radially stratified vortices in the limit of infinite Froude number. We thus turn our attention to vortex dynamics in inertial binary mixing flows, i.e. where two fluids of different densities are mixed in a flow unaffected by buoyancy forces. This has implications in mixing flows such as those encountered in combustion with non-premixed turbulent combustion depending strongly on the turbulent mixing of the fuel and oxidizer (e.g. Peters 2000). It is also relevant to basic mechanisms occurring in the interaction between the engine jet and the trailing vortices in an aircraft wake (Paoli, Laporte & Cuenot 2003). Large energy release by electric discharge due to lightning of laser-induced plasma discharge in the atmosphere have also been reported by Kurzweil, Livne & Meerson (2003) to exhibit baroclinic vorticity production and consecutive turbulent mixing of inhomogeneous fluids.

In two-dimensional turbulence, the formation of closed streamline patterns yields vortex cores trapping unmixed species. As noted by Cardoso *et al.* (1996) from quasi-two-dimensional experiments, the residence time of the fluid sample within the vortex core is thus close to the vortex lifetime. This, in turn, depends on strong vortex interactions among which the merger is responsible for fluid ejection and mixing, see Rogberg & Dritschel (2000) for the passive scalar case. While some approaches in this field are concerned with the statistical and spectral properties of the flow (Sandoval 1995; Bretonnet, Joly & Chassaing 2002), we focus here on the vortex dynamics and the description of elementary events relevant to the mixing efficiency of density-contrasted fluids.

The stability analysis of isolated vortices in Joly, Fontane & Chassaing (2005) have shown the robustness of low-density vortices and the receptivity of high-density vortices to perturbations consecutive to a Rayleigh–Taylor instability. As concluded in this paper, this instability alone may result in mass segregation by vorticity in a turbulent context. Work on inhomogeneous two-dimensional turbulence by Joly (2002 and ongoing) yields that turbulence evolves toward a dominant population of vortices containing light fluid and only a few vortices carrying heavy fluid. It proves also that vortex interactions play a major role in the mass-segregation mechanism together with the Rayleigh–Taylor instability. Among all possible interactions between two vortices, we limit our attention to the binary interaction between two similar co-rotating vortices sharing the same density stratification. More specifically, we examine how the critical merger is affected by the density ratio between the vortex core and its irrotational counterpart. The effects of asymmetries in the circulation between the two vortices will be addressed in subsequent work.

The paper is organized as follows. Section 2 presents the formulation of the equations governing the flow and provides details of the numerical algorithm. It also discusses the effects of the periodic boundary conditions on the interaction. Section 3

contains the main results of the study. We first revisit the influence of the Reynolds number on the interaction between the two vortices in the homogeneous case. Then we address the influence of the Atwood number, which measures the density contrast, on the critical merger distance. We show that light vortices in a heavy counterpart are more likely to merge than heavy vortices in a light counterpart. We next provide a simplified model based on an analysis of the effect of the baroclinic torque which redistributes vorticity due to the misalignment of the local acceleration of the fluid particles and the density gradient in the inhomogeneous case. Our conclusions and perspectives are given in § 4.

2. Formulation

2.1. *Basic equations*

We consider the binary mixing of two species of density ρ_c and ρ_b, respectively, in the vortex core and in the background fluid. By denoting $\Delta\rho = 0.5(\rho_c - \rho_b)$ the scale for the density difference and $\rho_m = 0.5(\rho_c + \rho_b)$ the mean density, the density contrast is the so-called Atwood number $At = \Delta\rho/\rho_m$. This parameter comes out as the fundamental measure of inertia effect in the dimensionless momentum and vorticity equations. An infinitely light vortex core corresponds to $At = -1$ whereas $At = 1$ is for infinitely heavy vortices.

In the limit of zero Mach number, the density of any fluid particle can be related to the mass fraction of the core fluid, denoted by C, according to $1/\rho = C/\rho_c + (1 - C)/\rho_b$ (see Bird, Stewart & Lightfoot 1960, on this point and for the mass fraction transport equation herein). Denoting $\mathscr{D}$ the Fickian diffusivity of the core fluid into the background one, and D_t the material derivative, the concentration equation is a pure advection–diffusion equation,

$$\rho\,\mathrm{D}_t C = \nabla\cdot(\rho\mathscr{D}\nabla C). \tag{2.1}$$

It is associated with the standard continuity equation:

$$\mathrm{D}_t\rho + \rho\nabla\cdot\boldsymbol{u} = 0. \tag{2.2}$$

When combining (2.1), (2.2) and the differentiated equation of state, it is found that the non-solenoidal part of the velocity field is of a diffusive nature (see Joseph 1990; Sandoval 1995)

$$\nabla\cdot\boldsymbol{u} = -\nabla\cdot\left(\frac{\mathscr{D}}{\rho}\nabla\rho\right). \tag{2.3}$$

We assume constant diffusivities such that the divergence of the velocity field reads $\nabla\cdot\boldsymbol{u} = -\mathscr{D}\Delta(\ln\rho/\rho_b)$. Denoting $\varrho = \ln(\rho/\rho_b)$, the velocity field may be written according to the Hodge decomposition $\boldsymbol{u} = \boldsymbol{v} - \mathscr{D}\nabla\varrho$ where $\nabla\cdot\boldsymbol{v} = 0$. As such, it can be viewed as the combination of a solenoidal advection field and a pure dilatational one resulting from mass diffusion. Assuming constant diffusivities biases the flow at dissipative scales. These scales are essentially seen in the vorticity filaments generated during the vortex interaction. These filaments are almost passively advected and are irrelevant to the large-scale interaction leading to the vortex merger.

For the description of the density field we retain the dimensionless transport equation for the modified density ϱ,

$$\mathrm{D}_t\varrho = (ReSc)^{-1}\Delta\varrho, \tag{2.4}$$

and the dimensionless constraint $\nabla\cdot\boldsymbol{u}=-(ReSc)^{-1}\Delta\varrho$, where Re and Sc are, respectively, the Reynolds and Schmidt numbers. The Reynolds number is defined as $Re=\Gamma/\nu$ where Γ is the circulation of one vortex and ν is the kinematic viscosity. We take $Sc=\nu/\mathscr{D}=1$. Let a_0 be the initial characteristic radius of the vortex cores. We denote by g' the projection of the gravity field onto the vortex plane. We thus form the vortex Froude number $Fr=(\Gamma/a_0)/\sqrt{Ata_0g'}$ and consider $Fr\gg 1$. The dimensionless momentum equation reads

$$\mathrm{D}_t\boldsymbol{u}=-\frac{1}{\rho}\nabla p+Re^{-1}\Delta\boldsymbol{u}. \tag{2.5}$$

Denoting $\pi=p/\rho$ the specific pressure, the corresponding dimensionless vorticity equation reads

$$\mathrm{D}_t\omega=-At\nabla\pi\times\nabla\varrho+\frac{1}{Re}\Delta\omega. \tag{2.6}$$

It is seen that the baroclinic torque on the right-hand side of the vorticity equation scales with the Atwood number.

2.2. *Numerics*

The density equation (2.4) and the momentum equation (2.5) are advanced in time using a third-order Runge–Kutta scheme. During each step of the scheme, we use a projection method (see Chorin 1969; Bell, Colella & Glaz 1989) transposed to the variable-density situation. The equations are first recast in the form

$$\partial_t\varrho=\underbrace{-(\boldsymbol{u}\cdot\nabla)\varrho+(ReSc)^{-1}\Delta\varrho}_{\boldsymbol{A}}, \tag{2.7a}$$

$$\partial_t\boldsymbol{u}=-\nabla\pi_h+\underbrace{\omega\times\boldsymbol{u}-\pi\nabla\varrho+Re^{-1}\Delta\boldsymbol{u}}_{\boldsymbol{B}}, \tag{2.7b}$$

where $\pi_h=\pi+\boldsymbol{u}^2/2$. Then we use a three-step procedure to evaluate the estimated density and velocity fields at the next substep t_+

$$\varrho^{t_+}=\varrho^t+\int_t^{t_+}\boldsymbol{A}\,\mathrm{d}t,\quad \boldsymbol{u}^*=\boldsymbol{u}^t+\int_t^{t_+}\boldsymbol{B}\,\mathrm{d}t, \tag{2.8a}$$

$$\Delta\pi_h^{t_+}=\frac{1}{\Delta t}[\nabla\cdot\boldsymbol{u}^*-(ReSc)^{-1}\Delta\varrho^{t_+}], \tag{2.8b}$$

$$\boldsymbol{u}^{t_+}=\boldsymbol{u}^*-\Delta t\nabla\pi_h^{t_+}. \tag{2.8c}$$

The velocity divergence is consistent with the density field since, by construction, $\nabla\cdot\boldsymbol{u}^{t_+}=-(ReSc)^{-1}\Delta\varrho^{t_+}$. As reported by Nicoud (1998) who adopted a similar approach in low-Mach-number thermal-mixing flows, the Poisson equation (2.8*b*) ensures that the divergent-free constraint is recovered in the inviscid limit. The time step is variable and adjusted according to the current maximum of velocity ensuring the Courant–Friedrichs–Lewy condition is respected with $CFL=\Delta t/\Delta x\times\max(u)$ kept under 0.7.

This procedure is implemented within the frame of a pseudospectral code dealiased according to the two-thirds rule. The flow is thus doubly periodic in contradiction with the targeted boundary conditions consisting of an unbounded domain with non-zero circulation where the vortices evolve. It is known (see Pradeep & Hussain 2004) that the biperiodic conditions result in a background negative vorticity ω_b that cancels with the positive net circulation of the vortex flow. This background vorticity

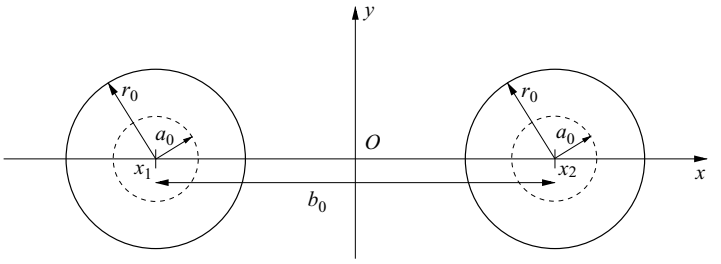

FIGURE 1. Configuration of the initial conditions with b_0 the initial separation between vortex centres, r_0 the truncation radius of the vortex and $a_0 = (J/\Gamma)^{1/2}$ the initial radius of the vortex core.

decreases while decreasing the ratio of vortex size to width of the square calculation domain. Let L_d be the width of the domain and Γ the individual circulation of each vortex in the pair, then $\omega_b = -2\Gamma/L_d^2$. The influence of this numerical artefact on the kinematics and merger time of the vortex pair is further discussed in the Appendix.

2.3. *Initial conditions*

Following Meunier *et al.* (2002) who studied the merger of uniform-density two-dimensional vortices, we use as initial conditions two truncated Gaussian vortices. Gaussian distributions of vorticity are commonly observed during the early stages of two-dimensional turbulence (see Jimenez, Moffatt & Vasco 1996). On the other hand, it was shown by Legras, Dritchel & Caillol (2001) that vortices would be naturally eroded, losing the weak peripheral vorticity, resembling truncated Gaussian vortices. The vorticity of each individual vortex is

$$\omega = \beta \exp\left(-\alpha \frac{r^2}{r_0^2}\right) \quad \text{if} \quad 0 \leqslant r \leqslant r_0, \tag{2.9}$$

with

$$\beta = \frac{\Gamma \alpha}{\pi r_0^2 (1 - \exp(-\alpha))}, \tag{2.10}$$

where r is measured from the centre of each vortex

The ratio between the minimum vorticity at the truncation radius r_0 and the maximum vorticity at the vortex centre is given by $\omega_{min}/\omega_{max} = \exp(-\alpha)$. We take $\alpha = 3$ for which $\omega_{min}/\omega_{max} = 0.05$. Each vortex is also characterized by its angular impulse $J = \iint_S \omega(r) r^2 \, \mathrm{d}s$ in the polar coordinate system attached to the vortex centre.

Meunier *et al.* (2002) introduce a length scale $a = (J/\Gamma)^{1/2}$ which is used to normalize the critical merger distance between two-dimensional uniform-density vortices. This length scale is shown to be the relevant one and allows us to define a universal criterion for the merger. In the situations described above for homogeneous vortices, Meunier *et al.* (2002) showed that the critical merger distance corresponded to $a/b \simeq 0.22$. For the particular case with $\alpha = 3$ we have $r_0/a_0 = 1.887$. If far enough from each other, the vortices evolve with an individual characteristic advective time scale $\tau = 2\pi a^2/\Gamma$ and a viscous time scale $\tau_\nu = \tau Re$. The spreading rate of the vortex core radius a by molecular diffusion is $a^2 = a_0^2 + 4\nu t$. The vortex pair is sketched in figure 1. For large separation distances, it will revolve in time according to the turnover time scale $T_0 = 2\pi^2 b_0^2/\Gamma$ corresponding to the turnover period of a pair of point vortices with the same circulation Γ and initial separation b_0.

	Homogeneous			Vortices with a light core						Vortices with a heavy core				
Run	H1	H2	H3	L1	L2	L3	L4	L5	L6	D1	D2	D3	D4	D5
At	0	0	0	$-\frac{4}{5}$	$-\frac{2}{3}$	$-\frac{1}{2}$	$-\frac{1}{2}$	$-\frac{1}{2}$	$-\frac{1}{5}$	$\frac{1}{4}$	$\frac{1}{2}$	$\frac{1}{2}$	$\frac{1}{2}$	$\frac{2}{3}$
b_0/r_0	2.6	2.9	3.6	2.9–3.1		2.6	2.9	3.6	2.8–3.0	2.7–2.9	2.6	2.9	3.6	2.0–2.1
Re	10^3–10^4			6000		10^3–10^4			6000	6000	10^3–10^4			6000

TABLE 1. The relevant parameters of the numerical simulations. Simulations are performed using a 512^2 grid, except for cases H3, L5 and D4 for which the resolution is increased to 1536^2. The proportion of the width of the vortex pair to the domain width is kept constant with $h = (b_0 + 2r_0)/L = 1/\pi$.

We superimpose on each vortex a Gaussian radial density distribution. Without loss of generality, we set ρ_b to 1 and ρ_c is set according to the Atwood number. The density distribution of each vortex reads

$$\rho = 1 + (\rho_c - 1)\exp\left(-\alpha \frac{r^2}{r_0^2}\right). \tag{2.11}$$

We do not truncate the density distribution to preserve bounded values for the density gradient at the vortex boundary. These initial conditions correspond to a couple of barotropic vortices with circular isopycnals and circular streamlines implying no initial baroclinic torque. The density is distributed radially on the same characteristic radius as the vorticity. The Gaussian distribution of density within the vortices stems from the self-similarity of density and vorticity profiles spreading by diffusion with a unit Schmidt number. According to the stability analysis derived by Joly *et al.* (2005), isolated heavy vortices of equivalent density and vorticity radii are stable to the Rayleigh–Taylor instability up to an Atwood number of 0.5.

2.4. *Numerical simulations*

According to the tests detailed in the Appendix, all the simulations are carried out on a 512^2 grid with $h = 1/\pi$. The ratio of the initial separation distance to the truncation radius b_0/r_0, the Reynolds number $Re = \Gamma/\nu$ and the Atwood number may be varied independently. We measure the time evolution of the distance b between the two vortices. This distance corresponds to the distance between the two local extrema of the streamfunction ψ which indicate the centre of each vortex. We define a 'merger time' t_f, which corresponds to the time elapsed until b decreases to a fraction f of the initial separation b_0, i.e. $b(t_f)/b_0 = f$.

First, we demonstrate the ability of the numerical method to catch the Reynolds-number dependence of the merger time in the homogeneous reference case. Then, defining a time horizon, we apply a simple merger criterion to illustrate the effect of the density contrast on the critical distance for a given Reynolds number. Reynolds-number sensitivity is also accounted for as we extend the definition of the critical separation distance to the variable-density situation. Table 1 gives the list of the simulation parameters that are used herein. High-resolution cases on a 1024^2 grid are carried out at least in order to detail the short-term development of the flow and study the impact of baroclinic sources of vorticity on the distance between vortex centres.

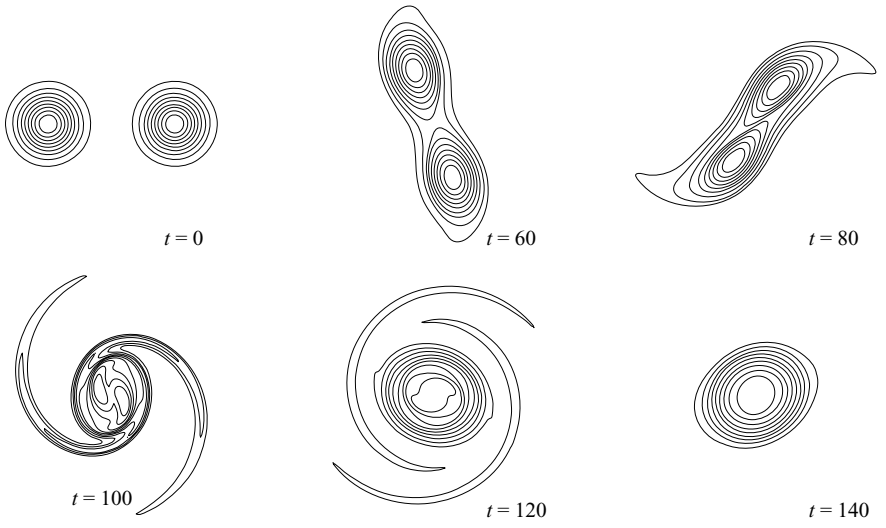

FIGURE 2. Sequence of vorticity contours for the case H1 with $(At, Lc/r_o) = (0, 2.6)$ and $Re = 6000$. Time in advective units. Contour every $\omega_{max}/10$ where ω_{max} is the instantaneous maximum vorticity.

3. Results

3.1. *The merger in the homogeneous case*

The merger in the homogeneous case H1 is shown in figure 2 from the contours of vorticity. As expected, we observe a viscous spreading of the vortices followed by a strong vortex interaction during which vortices merge from their inner edges and generate filaments of vorticity which are eventually dissipated. Note that in this case, $a/b_0 = 0.204$ initially. We have investigated the effects of the Reynolds number in the inhomogeneous situation according to the merger criterion derived by Meunier *et al.* (2002). As the Reynolds number is increased, the viscous spreading is slowed down and it takes longer for the vortices to reach the strong interaction regime referred to as the convective merger. Using the viscous spreading of an isolated Gaussian vortex, $a^2 = a_0^2 + 4\nu t$, we can define a time origin where the vortex is a point vortex as $t_0 = -a_0^2/4\nu$. Following Meunier *et al.* (2002), we define a non-dimensional time $t^* = (t - t_0)/T_0$ such that the viscous spreading of the vortex is now represented by

$$a^2 = \frac{8\pi^2 b_0^2}{Re} t^* \quad \text{or} \left(\frac{a}{b_0}\right)^2 = \frac{8\pi^2}{Re} t^*. \tag{3.1}$$

Hence the non-dimensional critical merger time $t_c^* = ARe$, where $A = (a/b_0)_c^2/8\pi^2$, depends linearly to Re.

An additional time period B_f is required in the pure convective merger interaction stage for the separation distance to collapse to a given fraction f of the initial separation b_0. This additional time depends only on the fraction f such that the overall non-dimensional time to reach the condition $b/b_0 = f$ reads

$$t_f^* = ARe + B_f. \tag{3.2}$$

From figure 3, we investigate the influence of the choice of f in the determination of the critical ratio $(a/b_0)_c$. We see that results converge as long as f is taken to be less than 0.4, and we find that the critical merger distance for the homogeneous

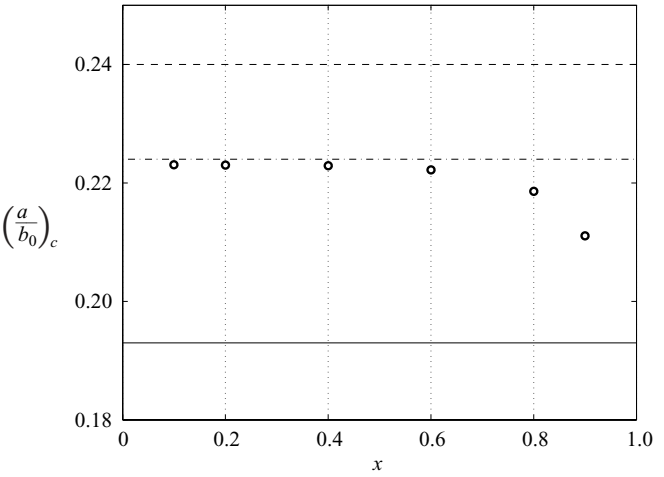

FIGURE 3. Influence of the fraction distance x on the critical ratio of the vortex radius to the separation distance. —, theoretical prediction for distributed truncated vortices with $\alpha = 3$ according to Meunier *et al.* (2002); - - -, experimental value from the same authors; –·–, theoretical prediction for uniform vortex patches according to Saffman & Szeto (1980); ○, results from direct viscous simulations.

case $\simeq 0.22$. The discrepancy with the results from other authors reported in the figure is due to the difference of the approaches as mentioned in § 1. The result was not straightforward since, in a preliminary stage, the viscous spreading proceeds together with a mutual adaptation of the vortices. Indeed, our initial conditions do not consist of a pair of steadily rotating vortices, but axisymmetric vortices. Contrary to the homogeneous situation, we are not able to define an equilibrium state for a pair of radially stratified vortices. Hence, and for all cases, we start from a simple axisymmetric configuration. In the homogeneous case, when the simulation starts, vortices deform tending to relax to the (unstable) equilibrium. Similar deformations are also seen at early stages of the interaction of radially stratified vortices. In the stratified cases, these deformations break the barotropy of the vortices, and induce a baroclinic production/destruction of vorticity.

3.2. *Effect of At on the critical distance*

Among all simulations performed, we first select three cases to illustrate the consequences of the inhomogeneous density field. The Reynolds number Re is set to 6000. The initial separation distance is $b_0/r_0 = 2.6$, or $a_0/b_0 = 0.204$. The Atwood number is, respectively, set to 0, -0.5 and 0.5 for the homogeneous H1, the light L3 and the dense D2 initial conditions. Figure 4(a) shows the time evolution of the vortex separation in advective time units. The merger of homogeneous vortices completes after 80 advective time units or equivalently after one turnover period T_0. We also see from figure 4(a) that the merger of light vortices occurs much sooner and completes by $t = 40\,\tau$ (case L3). Conversely, the complete merger of vortices is delayed until $t = 200\tau$ in case D2, i.e. if the vortex core is initially three times denser than the background irrotational fluid. Moreover it is observed that for heavy vortices, the early interaction yields a slight increase of the separation distance. The underlying inertia effects are thus favouring the merger of light vortices while initially preventing the onset of a convective merger interaction between heavy vortices.

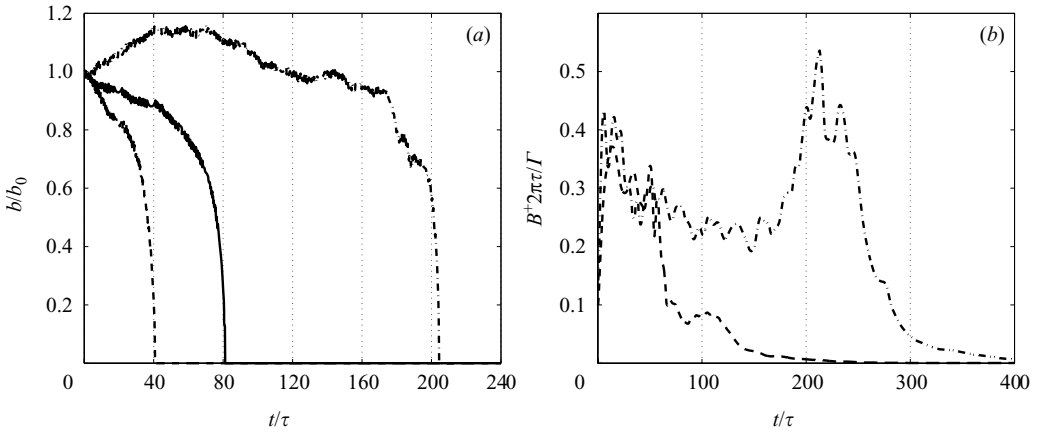

FIGURE 4. (*a*) Temporal evolution of vortex separation b/b_0 for $b_0/r_0 = 2.6$; (*b*) evolution of the net production of positive vorticity. Homogeneous vortices case H1 (solid line), light vortices case L3 (dashed), dense vortices case D2 (dot-dashed).

We integrate the net production of positive or negative vorticity over the domain. This provides the instantaneous integral over the domain of the positive contribution of the baroclinic torque to the vorticity budget

$$B^+ = \iint_D \left(-\frac{1}{\rho}\nabla p \times \nabla\varrho\right)^+ \mathrm{d}s.$$

This net source of positive vorticity is exactly balanced by a source of negative vorticity. It is normalized here by $\Gamma/2\pi\tau$ and shown in figure 4(*b*) beyond the merger time and until a full merger completes with relaxation to a stable axisymmetric vortex. The baroclinic vorticity generation is seen to rise immediately after the beginning of the simulation in response to the mutual deformation of the otherwise barotropic initial conditions. It then decreases slowly during the viscous stage while diffusion spreads the vortex cores and smoothes density gradients. The convective merger yields large deformations and associated large contributions of the baroclinic torque to the vorticity budget. We thus have a unique scenario for both light and heavy vortex mergers displaying two stages. When interacting from a small enough distance, heavy and light vortices exhibit opposite responses to their mutual deformation. During this first stage, diffusion spreads vortex cores and smoothes density gradients. They eventually merge in a second stage. In the case of light vortices, the first stage hastens the merger whereas in the heavy case, diffusion of mass excess in the vortex cores turns out to be a prerequisite to the convective merger. The convective mergers of both light and heavy vortex pairs involve large vorticity sources.

From the sequence of density contours in figure 5, we see that the merger of light vortices proceeds from a classical route. The interaction first deforms the scalar contours that are connected from their inner sides, $t = 20, 40$. Then the merger of the vortex cores follows and it is more pronounced at the same stage when $t = 60$ than in the homogeneous situation, compared with figure 2 at $t = 100$. During this core merger, strained density filaments are expelled from the core together with vorticity filaments, and are eventually dissipated as in the standard scenario. Axisymmetrization of the resulting slightly larger light vortex ultimately produces a stable barotropic vortex. The short-term interaction of heavy vortices is shown in figure 6. Their

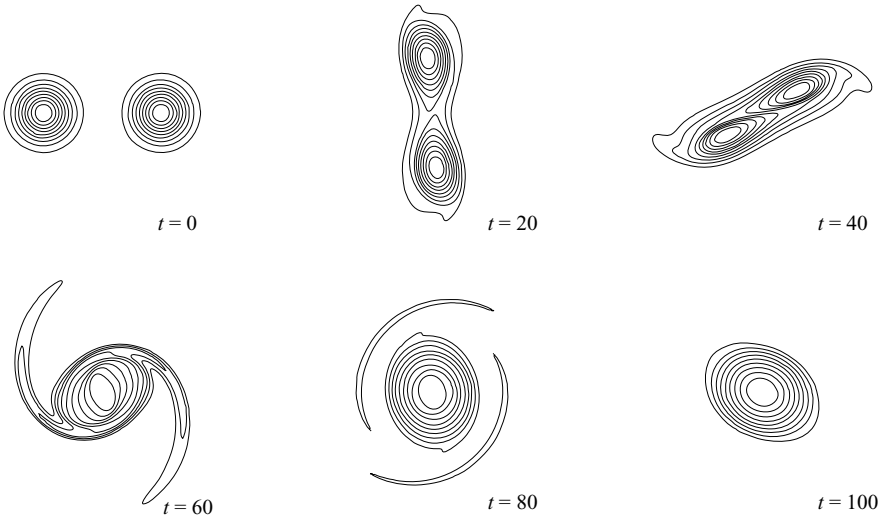

FIGURE 5. Sequence of density contours for the case L3 with $(At, Lc/r_o) = (-0.5, 2.6)$. Time in vortex units $\tau = \Gamma/2\pi a_0^2$. Contour every $(\rho_{max}/\rho_{min})/10$.

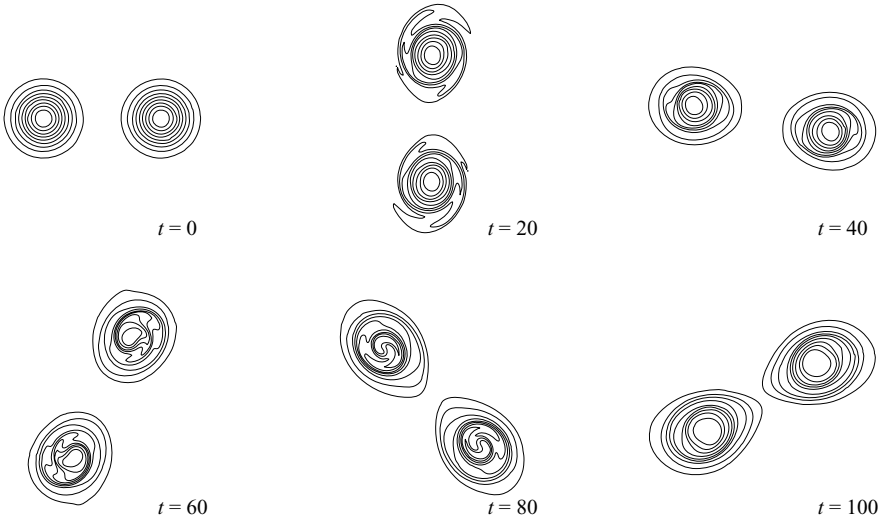

FIGURE 6. Sequence of density contours for the case D2 with $(At, Lc/r_o) = (0.5, 2.6)$. Time in vortex units $\tau = \Gamma/2\pi a_0^2$. Contour every $(\rho_{max}/\rho_{min})/10$.

interaction results in a small increase of the separation distance correlated with an ongoing adaptation of vorticity sources in response to the loss of barotropy. These sources, analysed later, are responsible of the particular topology of the advection field, both preventing any convective merger, and distorting density contours. During this phase of mutual repulsion, the vortex deformations and small-scale distortions are promoting viscous diffusion. By $t = 100$, when the separation distance $b(t)$ has decreased back around its initial value b_0, the repulsive effect of baroclinic vorticity sources has been damped and no longer prevents a convective merger (figure 4*a*).

In the perspective of vortex interactions in a two-dimensional turbulence context, we first address the effect of the Atwood number for a fixed Reynolds number $Re = 6000$

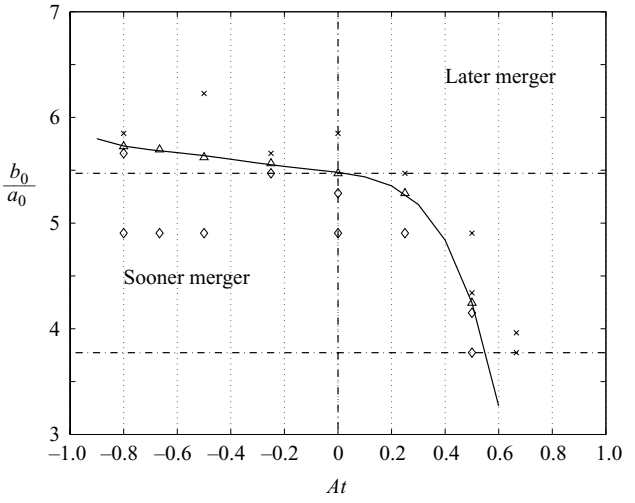

FIGURE 7. Sensitivity of the merger time to the Atwood number for a fixed Reynolds number $Re = 6000$. Cases from table 1 with varying initial separations and Atwood numbers are compared to a reference homogeneous case with initial separation $b_0/a_0 = 5.5$ or $b_0/r_0 = 2.9$ yielding a full merger for a time horizon $t_h = 160\tau$. Vortices merging sooner than t_h ($\diamond$), vortices merging later than t_h ($\times$) and vortices merging at t_h ($\triangle$—).

by considering the merger time relative to a reference time horizon $t_h = 160\tau$. This time horizon corresponds to the complete merger time of an homogeneous vortex pair with initial separation $b_0/r_0 = 2.9$, case H2 with $Re = 6000$. Towards this reference case, a complete merger can occur sooner or later in response to variations of the initial separation distance or to non-zero Atwood numbers. This leads to a simple representation of the inertia effects on the critical separation distance b_0/a_0 detailed in figure 7 based on a comprehensive analysis with Atwood numbers spanning from $-4/5$ to $2/3$. Light vortices for negative Atwood numbers are seen to interact strongly from larger separation distances than the homogeneous vortex pair. Heavy vortices do not merge before t_h unless falling within small interaction distances. According to the prescribed time horizon, no merger can occur within this time horizon for Atwood numbers above 0.6 even if placed in contact on their inner sides, i.e. for $b_0 \to 2r_0$ which corresponds here to $b_0/a_0 \to 3.77$. From this first inspection, it can be inferred that the probability of a merger event between heavy vortices in binary-mixing two-dimensional turbulence will be much lower than for light vortices.

We then analyse the influence of the Reynolds number on the stage preceding the convective merger. The normalized merger time $t^*_{0.4} = (t_{0.4} + a_0^2/4\nu)/T_0$ is found in figure 8(a) to increase linearly with the Reynolds number even for $At \neq 0$. The difference between the homogeneous and the inhomogeneous merger lies on the nonlinear vorticity baroclinic source. Yet, it is still found that the length of the initial stage preceding the convective merger grows linearly with the Reynolds number for a given Atwood number. Hence, the time delay added or subtracted before the onset of the convective merger owing to the non-viscous baroclinic vorticity production is still affected linearly by mass diffusion. Given a unit Schmidt number, we verify only that mass diffusion decreases density gradients (and corresponding baroclinic vorticity sources) on the same time scale as momentum diffusion spreads the vortex cores.

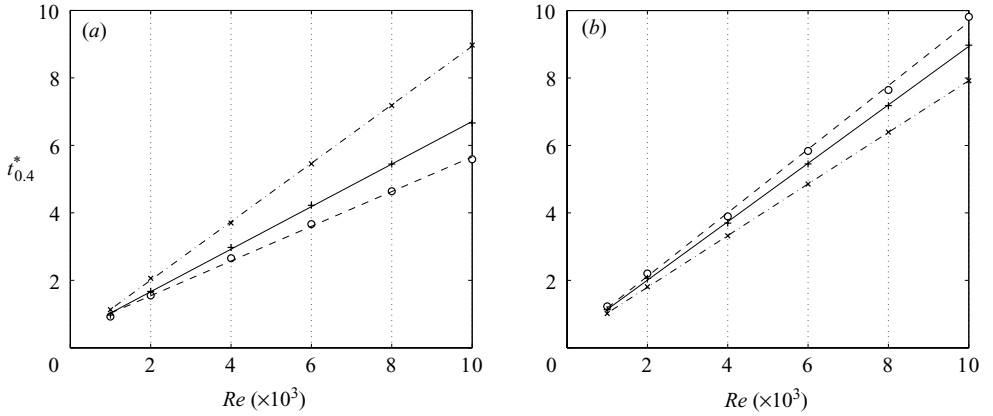

FIGURE 8. (*a*) Merger time $t^*_{0.4}$ versus vortex Reynolds number for a fixed initial distance $b_0/r_0 = 2.9$ in the homogeneous case H2 (——), light vortices case L4 (- - -) and dense vortices case D3 (——·——). (*b*) Merger time $t^*_{0.4}$ versus vortex Reynolds number for a fixed Atwood number $At = 0.5$ and varying initial distance D2 with $b_0/r_0 = 2.6$ (- - -), D3 with $b_0/r_0 = 2.9$ (——) and D4 with $b_0/r_0 = 3.6$ (——·——).

The linearity of the response of $t^*_{0.4}$ to the Reynolds number has been checked to hold over the whole range of tested Atwood numbers. It motivates the use of the procedure derived by Meunier *et al.* (2002) to measure a critical distance for radially stratified vortices. However, contrary to the homogeneous case, the initial separation still has an influence on slope A. It is shown in figure 8(*b*) where the normalized merger time $t^*_{0.4}$ is plotted against the Reynolds number for three different initial separations ($b_0/r_0 = 2.6, 2.9, 3.6$) and a single Atwood number, $At = 0.5$. We find three different slopes with the steepest associated to the pair of vortices initially closer, the slope of initially remote vortices being shallower. While the merger time still grows linearly with the Reynolds number, the additional mechanism associated with the loss of barotropy depends on the amplitude of the initial deformation. For initially close vortices, this deformation is large owing to the strong difference between the pair of axisymmetric vortices and the homogeneous equilibrium state. In this case, the bias on slope A resulting from the density stratification is large since, at the beginning of the strong merger interaction, the stratification is also close to the initial one. On the opposite and for initially remote heavy vortices, the initial deformation is small since a pair of remote axisymmetric vortices is close to an equilibrium state. Moreover, the merger interaction begins after a preliminary diffusion stage has eroded the density contrast. Both mechanisms reduce the baroclinic vorticity sources and the slope A tends to be closer to the one obtained with no stratification. Since the critical distance $(a/b_0)_c$ associated to the measure of slope A depends on the initial distance b_0, we conclude that there is no universal measure of the critical distance associated to a given Atwood number.

Moreover, we find that the purely diffusive spreading of the vortex cores is only observed for vortices which are initially well separated. In these cases, the deformations of the vortices induced by their straining fields are weak and the vortices remains mainly barotropic, hence the baroclinic torque is negligible at these initial stages. For closer vortices, the large initial deformation and the baroclinic vorticity redistribution significantly alter the evolution of the core size $a = \sqrt{J/\Gamma}$. If $b_0/r_0 = 2.9$, we see from figure 9(*a*) that massive (resp. light) vortices initially shrink (resp. dilate) in response to the loss of barotropy during their rapid mutual interaction. When the

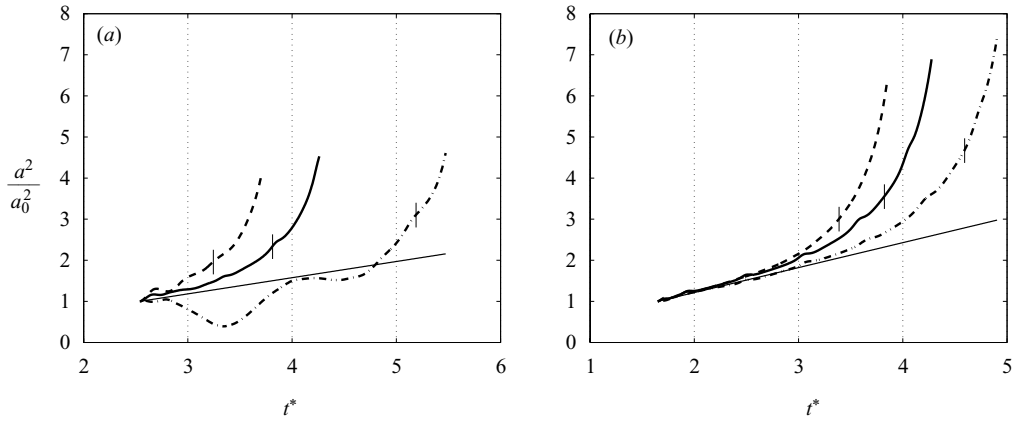

FIGURE 9. Evolution of the vortex core size $a = \sqrt{J/\Gamma}$ for $Re = 6000$ and (*a*) $b_0/r_0 = 2.9$; H2 (——), L4 (- - -), D3 (—·—) and (*b*) $b_0/r_0 = 3.6$; H3 (——), L5 (- - -), D4 (—·—). The linear slope corresponds to the diffusive spreading of the isolated vortex, $a^2/a_0^2 = 1 + (8\pi/Re)\ t/\tau$. Small vertical ticks mark the normalized critical merger time $t^*_{0.4} - B_{0.4}$.

initial distance is as large as $b_0/r_0 = 3.6$ (figure 9*b*), the vortex core spreads according to $a^2/a_0^2 = 1 + (8\pi/Re)\ t/\tau$ whatever the Atwood number. The convective merger thus occurs for $b_0/r_0 = 3.6$ after the simultaneous diffusion of mass and momentum. As derived in § 3.1, the measure of the critical distance from the slope A assumes a proper preliminary diffusion of the vortices. A virtual diffusive stage is embedded in the normalized merger time $t^* = (t - t_0)/T_0$ through the time origin $t_0 = -a_0^2/4\nu$. If not too close, vortices also undergo an actual diffusive spreading at the beginning of the simulation. This is necessary to ensure a correct use of slope A to obtain a measure of $(a/b_0)_c^2$ by $8\pi^2 A$. This condition is not fulfilled if $b_0/r_0 = 2.9$, and we can only acknowledge that the normalized merger time grows linearly with the Reynolds number. It is fulfilled if $b_0/r_0 = 3.6$ and, though specific of this initial separation, the critical distance $(a/b_0)_c^2$ deduced from slope A measures density effects made independent of the Reynolds number. The concept of a critical distance is weakened when $At \neq 0$ and should be understood in the following as being always dependent of the initial separation.

Figure 10 summarizes the sensitivity of the critical separation distance to the Atwood number measured for an intial distance $b_0/r_0 = 3.6$. Measurements of $\sqrt{8\pi^2 A}$ over the same range of Atwood numbers are also shown when $b_0/r_0 = 2.9$. The trend is the same as that discussed from the previous point of view based on a time horizon for a fixed Reynolds number. For negative Atwood numbers, the critical ratio $(a/b_0)_c$ decreases under the homogeneous threshold. Hence, for a given Reynolds number and an initial separation, light vortices strongly interact from larger distances than in the homogeneous situation. For positive Atwood numbers, the critical ratio $(a/b_0)_c$ increases steeply for a pair of vortices with increasing mass excess to the surrounding fluid. For initial separations below $b_0/r_0 = 3.6$, a critical distance is hardly defined for Atwood numbers above 0.6.

3.3. *Baroclinic sources of vorticity*

We now describe in more detail the vorticity distribution within the vortices at the early stages of the flow evolution to understand better the mechanism that triggers a rapid merger or slows it down. Since the only difference in the dynamics is the

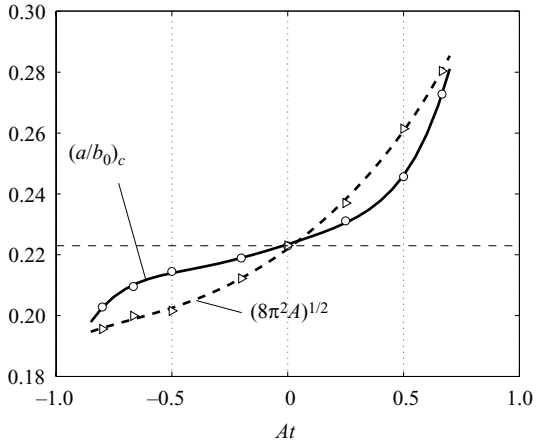

FIGURE 10. —, critical separation versus Atwood number for an initial distance $b_0/r_0 = 3.6$; - - -, $\sqrt{8\pi^2 A}$ versus Atwood number for initially close vortices $b_0/r_0 = 2.9$.

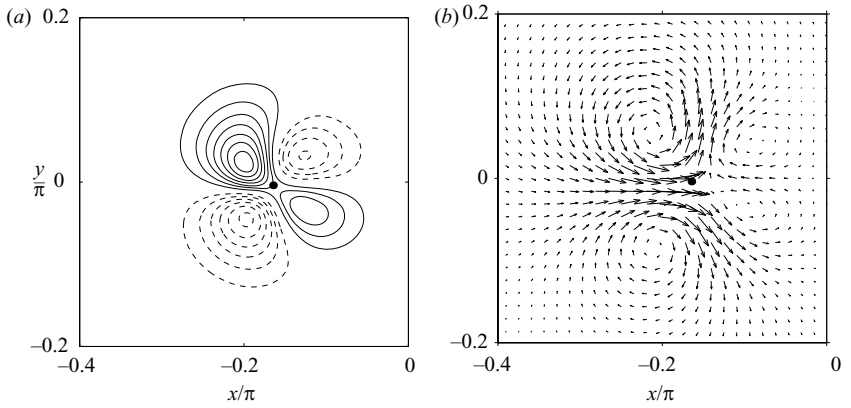

FIGURE 11. (*a*) Contours of the cumulative baroclinic vorticity ω_Δ and (*b*) induced velocity field, for $At = -0.5$ (low-density vortices) and $b_0/r_0 = 2.6$ at $t = 0.2\,\tau$. The black spot indicates the vortex centre.

baroclinic torque which is now active, we focus on the additional vorticity resulting from this source term. We denote as ω_Δ the vorticity field resulting from the difference between the vorticity of a passive scalar reference case and the vorticity of a current case with a full contribution of inertia effects. This vorticity difference corresponds to the vorticity accumulated between the initial state and the current time owing to the baroclinic sources or sinks:

$$\omega_\Delta = -\int_{particle\ path} \frac{1}{\rho}\nabla p \times \nabla\varrho \,\mathrm{d}t. \tag{3.3}$$

Note that at the limit of $Re \to \infty$, the pressure term $\nabla p/\rho$ is balanced by $\mathrm{D}_t\boldsymbol{u}$ such that the baroclinic torque is purely inertial, and is directly linked to the misalignment between the local acceleration of a fluid particle and the local density gradient. The contours of the cumulative baroclinic vorticity are shown in figure 11(*a*) on a single light vortex of the pair at an early stage of the interaction. The vortex displayed is initially the one at the left in the pair. The second vortex is the antisymmetric

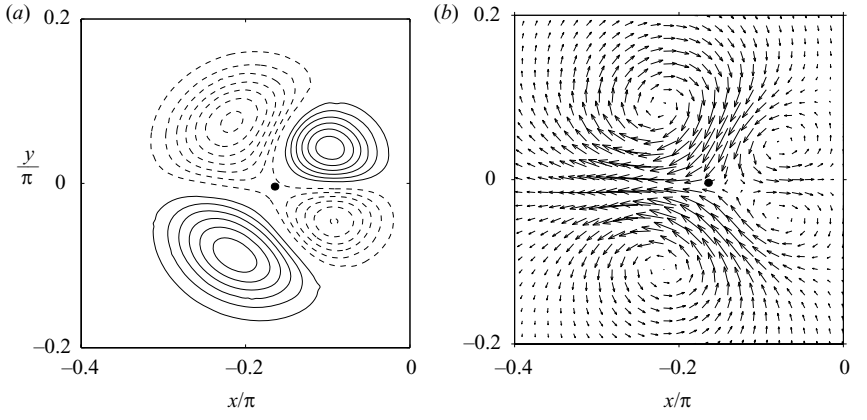

FIGURE 12. (*a*) Contours of the cumulative baroclinic vorticity ω_Δ and (*b*) induced velocity field, for $At = 0.5$ (high-density vortices) and $b_0/r_0 = 2.6$ at $t = 0.2\,\tau$. The black spot indicates the vortex centre.

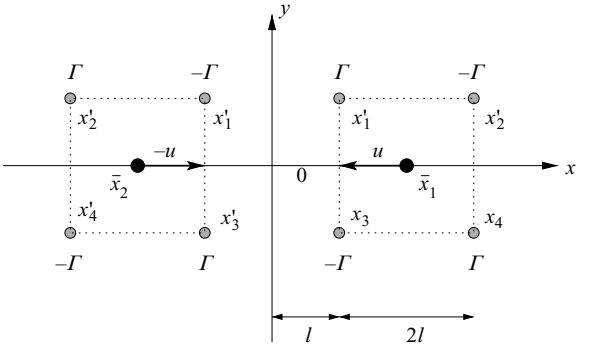

FIGURE 13. Sketch of the baroclinic quadrupoles.

image of this one. This additional contribution is seen to correspond to a quadrupole of alternately signed vortices. The formation of these quadrupoles by baroclinic effects follows the mechanism described by Joly *et al.* (2005) for deformed isolated vortices: the response to a deformation of a barotropic vortex on the azimuthal wavenumber m consists in a multi-pole distribution of alternate $2m$ vorticity sources and sinks. Here, the adaptation of each vortex to the strain field generated by the other one yields a deformation corresponding to $m = 2$. The two quadrupoles induce an additional velocity field (figure 11*b*) which brings the vortex centres closer to each other. Indeed, we see that the centre of the left-hand vortex is pushed to the right, and by antisymmetry the vortex on the right (not shown) is pushed to the left. For vortices denser than the background fluid (see figure 12), the signs of the poles of the dipoles are reversed and consequently, the velocity field induced by ω_Δ has a repulsing effect on the vortices. The vortices are pushed away from each other and cannot merge within one turnover time.

This observation can be easily explained using a simple model of equally distributed quadrupoles. The quadrupoles themselves consist of four point vortices. This simple configuration mimics the additional vorticity distribution observed in the numerical simulation. The geometry of the configuration is given in figure 13. We attach four

point vortices located at $(x_i')_{i=1,4}$ and of circulation $\pm\Gamma$ to the vortex on the left (vortex 2), and four point vortices located at $(x_i)_{i=1,4}$ to the vortex on the right (vortex 1). For reference, Γ is the circulation of the vortex located at x_1. All point vortices are regularly spaced. Although this choice is not generic, it is sufficient for a qualitative model. Let $\bar{x}_1$ be the geometrical centre of the quadrupole attached to vortex 1 and $\bar{x}_2$ be the geometrical centre of the quadrupole attached to vortex 2. From symmetry arguments, we can write $u_{\bar{x}_2} = -u_{\bar{x}_1}$. We then focus only on $u(\bar{x}_1)$. Moreover, the contributions from vortices (x_i) to $u_{\bar{x}_1}$ cancel (as well as contributions from x_i' to $u_{\bar{x}_2}$). The vertical antisymmetry makes the contributions of x_1' and x_3' equal, as well as the contributions of x_2' and x_4'. Thus, denoting the separation between vortices as 2ℓ, the velocity induced by the quadrupole x_i' on $\bar{x}_1$ is

$$u_{\bar{x}_1} = -\frac{4}{65\pi\ell}\Gamma. \tag{3.4}$$

For the pair of light vortices for which the circulation Γ is positive, the induced velocity field makes the centres $\bar{x}_1$ and $\bar{x}_2$ converge toward the centre of the system. The separation is increased for the high-density vortex pair associated with negative circulation. This simple model hence explains the phenomenon.

4. Conclusions

In this study we have investigated the merger of two co-rotating radially stratified two-dimensional vortices at high Reynolds number. Such a situation is relevant to the mixing of two fluids of different densities in industrial contexts. We first revisited the effects of viscosity on the merger of homogeneous vortices by direct numerical simulations. We carefully validated our numerical methods, taking particular care of the effects of the periodic boundary conditions imposed by our pseudospectral approach. Then, we confirmed the experimental results by Meunier *et al.* (2002) showing that the critical radii of the conditions for merger are $a/b_0 \simeq 0.22$ where a/b_0 is the ratio of the vortices to their separation distance. We also confirmed that the time required to enter the stage of convective merger depends linearly on the Reynolds number. This is indeed due to an initial viscous spreading of the vortices.

For the inhomogeneous cases, we also observed this linear dependence and it has been used to measure the critical value for a/b_0. We have shown that vortices carrying light fluid merge from a greater distance than do homogeneous vortices. On the contrary, vortices carrying heavy fluid must be much closer to merge, and when $At > 0.6$, the merger takes place only if the diffusion has significantly decreased the density gradients. These differences are associated with a vorticity production/destruction term, the baroclinic torque. The baroclinic torque is non-zero as far as the local acceleration misaligns with the density gradient. Here it is the case because the vortices, initially barotropic, deform one another from the start of the interaction. It is shown that on each vortex the baroclinic vorticity is organized at the early stages of the interaction as quadrupoles of alternate sign. The quadrupole attached to a vortex attracts or pushes away the second vortex and vice versa. In the case of light vortices, the vortices are attracted to each other. This decrease in their separation distance strengthens the interaction, and the vortices merge rapidly. On the other hand, in the case of heavy vortices, the added baroclinic vorticity quadrupole acts in the opposite way, increasing the distance between the vortices, and decreasing the strength of the interaction.

h	0.8	0.6	0.4	$1/\pi$	0.2	0.15	0.1
N	210	288	420	512	792	1120	1584

TABLE 2. Characteristics of the preliminary test varying the ratio $h = (b_0+2r_0)/L$ of vortex-pair width to calculation-domain width. Associated spatial resolution is $N_x \times N_y$ with $N_x = N_y = N$.

These results open avenues which are beyond the scope of this paper. A natural next question is, what is the influence of asymmetries in the initial conditions? In this study, we have limited attention to symmetric vortices to focus on the basic new phenomenology appearing with the density stratification. Yet it is known that even in the uniform density case, vortices of different circulation merge differently (see Dritschel 1995). In this case, we frequently observe partial merger, where more than one coherent structure results from the interaction. This open question is important since vortices of different circulation would naturally interact in complex flows such as turbulence. Another essential open question lies on the merger of vortices of unequal density stratification. For example, since it is shown that light vortices behave differently from heavy vortices, another asymmetry to be considered is the interaction between a light vortex and an heavy vortex in a medium counterpart. Finally, the study of the interaction between two three-dimensional columnar vortices and the emergence of three-dimensional modes is also to be explored.

Appendix. Controlling the effect of the boundary conditions

Considering the whole vortex system, we note that the distance between the outermost edges of the vortices is $b_0 + 2r_0$. We define $h = (b_0 + 2r_0)/L_D$, the ratio of the vortex-pair width to the domain width L_D. When focusing on binary-vortex interactions, we must confine the vortices well into the centre of the domain, i.e. take h to be small, to avoid the spurious influence of the periodic boundary conditions. Preliminary simulations are carried out in the homogeneous situation to validate a fair compromise between the computation cost and the sensitivity of the merger process to the parameter h. We preserve the spatial resolution of the vortex pair for a Reynolds number $Re = 6000$ and an initial separation distance $b_0 = 2.6r_0$. Corresponding grid sizes are given in table 2.

We first measure the turnover period of the pair of vortices by following one of the vortices during the first quarter of a turnover. We also measure the time evolution of the distance b between the two vortices. This distance corresponds to the distance between the two local extrema of the streamfunction ψ, which indicate the centre of each vortex. Finally, we measure a 'merger time' t_f, which corresponds to the time elapsed until b decreases to a fraction f of the initial separation b_0, i.e. $b(t_f)/b_0 = f$.

From figure 14(a), we conclude that the effective turnover period T is underestimated by $T_0 = 2\pi^2 b_0^2/\Gamma$ for a size ratio above $h = 1/\pi$. Equivalently it may be said that, owing to stringent boundary conditions, the numerical simulation fails to reproduce the kinematics of a point vortex pair for a size ratio above $h = 1/\pi$. The corresponding time evolution of the separation distance (figure 14b), is seen to depend strongly on h for $h > 0.4$. This is confirmed in figure 14(c), showing that t_f is unaffected provided $h < 0.4$. It is concluded that the merger is artificially favoured for $h > 0.4$ and insensitive to the periodicity of the flow for weaker confinement of the

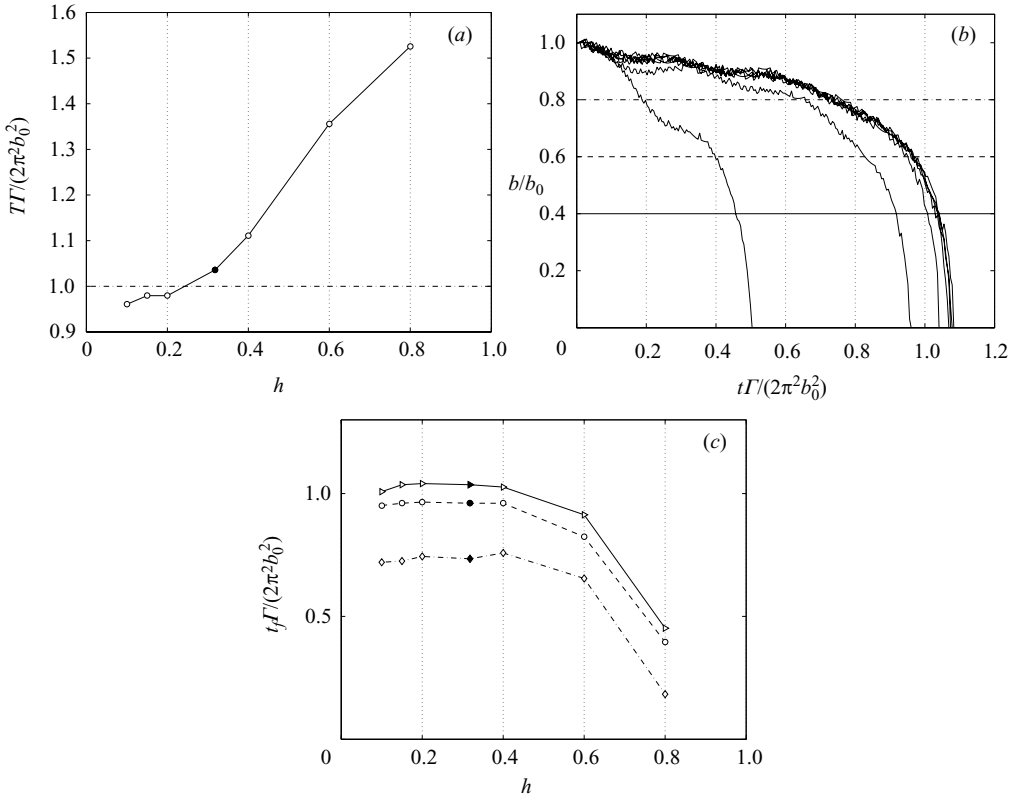

FIGURE 14. Influence of the periodic boundary conditions, on the merger process. (*a*) The turnover period T normalized by the turnover period of a point vortex pair $T_0 = 2\pi^2 b_0^2/\Gamma$. (*b*) Evolution of the separation distance with curves from left to right for decreasing h. (*c*) Merger time t_f measured for different fractions f of the separation distance: —, $f = 0.4$; – – –, $f = 0.6$; –·–, $f = 0.8$. Solid symbols in (*a*) and (*c*) are for $h = 1/\pi$ which is the compromise selected hereinafter.

vortex pair. We choose to set $h = 1/\pi$ both to retrieve an accurate turnover period and to measure a merger time insensitive to the width of the calculation domain.

REFERENCES

BELL, J. B., COLELLA, P. & GLAZ, H. 1989 A 2nd-order projection method for the incompressible Navier–Stokes equations. *J. Comput. Phys.* **85**, 257–283.

BIRD, R., STEWART, W. & LIGHTFOOT, E. 1960 *Transport Phenomena*. Wiley.

BRETONNET, L., JOLY, L. & CHASSAING, P. 2002 Direct numerical simulation of inertia sensitive turbulence. In *Eur. Turbulence Conf. 9*. Southampton, UK.

CARDOSO, O., GLUCKMANN, B., PARCOLLET, O. & TABELING, P. 1996 Dispersion in a quasi-two-dimensional-turbulent flow: an experimental study. *Phys. Fluids* **8** (1), 209–214.

CERRETELLI, C. & WILLIAMSON, C. 2003 The physical mechanism for vortex merging. *J. Fluid Mech.* **475**, 41–77.

CHORIN, A. J. 1969 On the convergence of discrete approximations to the Navier–Stokes equations. *Maths Comput.* **23**, 341–353.

DRITSCHEL, D. G. 1995 A general theory for two-dimensional vortex interactions. *J. Fluid Mech.* **293**, 269–303.

Dritschel, D. G. & Waugh, D. W. 1992 Qualification of the inelastic interaction of unequal vortices in two-dimensional vortex dynamics. *Phys. Fluids* A **4**, 1737–1744.

Jiménez, J., Moffatt, H. K. & Vasco, C. 1996 The structure of the vortices in freely decaying two-dimensional turbulence. *J. Fluid Mech.* **313**, 209–222.

Joly, L. 2002 Inertia effects in variable density flows. Habilitation à diriger des recherches, INPT, Toulouse.

Joly, L., Fontane, J. & Chassaing, P. 2005 The Rayleigh–Taylor instability of two-dimensional high-density vortices. *J. Fluid Mech.* **537**, 415–431.

Joseph, D. 1990 Fluid dynamics of two miscible liquids with diffusion and gradient stresses. *Eur. J. Mech.* B/*Fluids* **9**, 565–596.

Kurzweil, Y., Livne, E. & Meerson, B. 2003 Vorticity production and turbulent cooling of 'hot channels' in gases: three-dimensions versus two dimensions. *Phys. Fluids* **15** (3), 752–762.

Legras, B., Dritchel, D. & Caillol, P. 2001 The erosion of a distributed two-dimensional vortex in a background straining flow. *J. Fluid Mech.* **441**, 369–398.

Melander, M. V., Zabusky, N. J. & McWilliams, J. C. 1988 Symmetric vortex merger in two dimensions: causes and conditions. *J. Fluid Mech.* **195**, 303–340.

Meunier, P., Ehrenstein, U., Leweke, T. & Rossi, M. 2002 A merging criterion for two-dimensional co-rotating vortices. *Phys. Fluids* **14** (8), 2757–2766.

Meunier, P., Le Dizès, S. & Leweke, T. 2005 Physics of vortex merging. *C. R. Phys*. **6**, 431–450.

Nicoud, F. 1998 Numerical study of a channel flow with variable properties. *Center for Turbulence Res., Annu. Res. Briefs*, pp. 289–310.

Paoli, R., Laporte, F. & Cuenot, B. 2003 Dynamics and mixing in jet/vortex interactions. *Phys. Fluids* **15** (7), 1843–1860.

Peters, N. 2000 *Turbulent Combustion*. Cambridge University Press.

Pradeep, D. & Hussain, F. 2004 Effects of boundary conditions in numerical simulations of vortex dynamics. *J. Fluid Mech.* **516**, 115–124.

Rogberg, P. & Dritschel, D. 2000 Mixing in two-dimensional vortex interactions. *Phys. Fluids* **12** (12), 3285–3288.

Saffman, P. G. & Szeto, R. 1980 Equilibrium shapes of a pair of equal uniform vortices. *Phys. Fluids* **23** (12), 2339–2342.

Sandoval, D. 1995 The dynamics of variable-density turbulence. PhD thesis, University of Washington.

Waugh, D. W. 1992 The efficiency of symmetric vortex merger. *Phys. Fluids* A **4** (8), 1745–1758.